Analysis of post deposition processing for CdTe/CdS thin film solar cells

Brian E. McCandless and **Robert W. Birkmire**
Institute of Energy Conversion, University of Delaware, Newark, DE 19716 (U.S.A.)

(Received January 22, 1991)

Abstract

A post-deposition process for optimizing the efficiency of thin film CdTe/CdS solar cells deposited by physical vapor deposition has been developed and the effects of the individual process steps on the materials and device properties have been analyzed. A 400 °C heat treatment with $CdCl_2$ restructures the CdTe resulting in enhanced grain size and crystallographic reorientation. Structural and optical measurements indicate interdiffusion of sulfur and tellurium during the heat treatment resulting in formation of a CdS_xTe_{1-x} layer with a narrower band gap than CdTe. Bifacial current–voltage and quantum efficiency analysis of the CdTe devices at various stages of the optimization process shows the evolution of the device from a p–i–n structure to a heterojunction. A chemical treatment improves the open circuit voltage (V_{oc}) and Cu/Au contact to the CdTe. The optimization process can be applied to cells using CdTe and CdS deposited by different methods.

1. Introduction

High efficiency thin film CdTe-based cells have been prepared using CdTe deposited by a variety of methods such as close space vapor transport (CSVT) [1], electrodeposition [2], screen printing [3], organometallic chemical vapor deposition (OMCVD) [4] and molecular beam epitaxy (MBE) [5]. All thin film CdTe solar cells with efficiencies greater than 10% share three fabrication features: (1) a superstrate configuration; (2) a CdTe growth step or heat treatment step at 400 °C or greater; and (3) a CdTe contact containing copper or gold. With the exception of cells prepared by CSVT, the above processes utilized $CdCl_2$ in the preparation of the CdTe layer. The highest reported efficiencies for thin film CdTe cells are over 12% [6, 7]. Previously, we reported on a process for fabricating cells using evaporated CdTe films [8]. These devices utilized the three fabrication features and the devices typically had open circuit voltage (V_{oc}) < 0.650 mV and fill factor (FF) $= 65\%$ with short circuit current (J_{sc}) ≈ 20 mA cm^{-2}. The low FF was due in part to a poor contact to the CdTe. Device analysis showed that variations in FF were due to the light independent portion of the series resistance, which we attributed to interaction between the surface layer and the contact materials [9].

In this paper we present a process developed for optimizing evaporated CdTe cells for high efficiency. The optimization process and the changes resulting from each step on the material and device properties are discussed.

0379-6779/91/$3.50

2. Experimental details

The CdTe/CdS devices were prepared in a superstrate configuration as shown in Fig. 1. The devices were prepared by first sputter depositing 400 nm of ITO onto Corning 7059 glass, which had 95% transmission at 850 nm and a sheet resistance of 10 ohm per □. Undoped CdS films 1–2 μm thick were then deposited by physical vapor deposition (PVD) from an effusion source bottle using high purity CdS powder. The CdS films typically had a resistivity of 10 ohm cm^{-1}.

The CdTe films were also deposited by PVD using five–nine purity CdTe powder. Films 2 μm were deposited under the following conditions: bell jar base pressure, 1×10^{-5} Torr; substrate temperature, 250–300 °C; and CdTe growth rate, 0.1 μm min^{-1}.

Following the deposition, the CdTe surface was coated with a saturated $CdCl_2$:CH_3OH solution prepared by dissolving anhydrous $CdCl_2$ in CH_3OH at room temperature. The CH_3OH evaporated leaving a uniform precipitate of $CdCl_2$ in a manner similar to that described by Meyers *et al.* [10]. The samples were then heat treated in air at 400 °C for 30 min and rinsed in deionized water.

A semi-transparent Cu/Au contact (Cu ≈ 10 nm, Au ≈ 10 nm) was deposited onto the CdTe surface by electron beam evaporation and indium solder was used to form a robust contact to the ITO near each cell area. The device performance was optimized first by an air heat treatment at 150 °C for 30 min to 2 h to increase J_{sc}. Next, the samples were chemically treated by immersion in either 0.02 mol l^{-1} Br_2–CH_3OH for 5 s or in 95% N_2H_4–H_2O for up to 5 min to increase the V_{oc} and FF.

The surface morphology of the CdTe layers was examined by optical and scanning electron microscopy (SEM). Scanning X-ray diffraction (XRD) with 35 kV Cu Kα radiation and Bragg–Brentano focusing geometry was used to characterize the film structure. The precision lattice parameter, a_0, was determined by cubic reduction of each reflection and fitting to the Nelson–Riley–Taylor–Sinclair function [11]. Auger electron spectroscopic

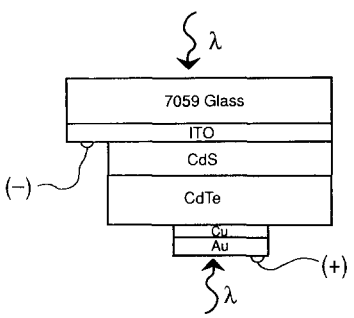

Fig. 1. Schematic cross-section of CdTe/CdS device in superstrate configuration with semi-transparent Cu/Au dot contact.

(AES), secondary ion mass spectroscopic (SIMS), and X-ray photoelectron spectroscopic (XPS) analysis were performed on samples of CdTe/CdS/ITO/glass films at each step of processing [12]. Total optical transmission T and reflection R were measured over the wavelength range 300 to 1400 nm using a Perkin–Elmer spectrometer with an integrating sphere and the absorption edge was estimated from plots of absorption (α) *vs.* energy.

Current–voltage (I–V) characteristics and quantum efficiencies (QE) were measured on completed solar cells through both the CdS and the semi-transparent Cu/Au contact. Illuminated I–V measurements were made using ELH lamp simulator.

3. Results and discussion

3.1. $CdCl_2$ heat treatment at 400 °C

As-deposited, evaporated CdTe films on CdS/ITO/7059 substrates are specular and deep gray in appearance, have submicron facets, and are moderately well oriented along the (111) axis. All XRD reflections for the as-deposited film are indexed as either the ITO substrate, the wurtzite CdS phase, or the zincblende CdTe phase and give a precision CdTe lattice parameter of 6.490 ± 0.005 Å. After coating with $CdCl_2$, the surface takes on the features of the $CdCl_2$ crystallites and exhibits a translucent white textured appearance.

Heat treatment at 400 °C and rinsing in deionized H_2O changes the surface appearance to milky and results in larger faceted morphology. SEM images show that the surface is comprised of facets of micron dimension. XRD scans indicate improved (111) orientation, sharpened CdTe reflections, and a reduction in the CdTe lattice parameter to 6.480 ± 0.005 Å. Additional heat treatment time results in further reduction in lattice parameter. This is consistent with interdiffusion of CdS and CdTe resulting in the formation of a mixed CdS_xTe_{1-x} layer and is supported by AES and SIMS results discussed below. Performing the 400 °C air heat treatment on a CdTe/CdS/7059 structure without a $CdCl_2$ coating results in a slight increase in orientation and no detectable change in lattice parameter or peak widths. However, heat treatment at >500 °C without $CdCl_2$ results in similar restructuring to the CdTe heat treated with the $CdCl_2$, suggesting that $CdCl_2$ acts as a recrystallizing agent.

Films grown by electrodeposition treated in the same manner show similar structural changes. In addition, the as-deposited films contain a tellurium phase which is removed by the 400 °C heat treatment with $CdCl_2$. Table 1 summarizes the change in the lattice parameter, a_0, the (111) peak intensity I and the (111) peak widths, full width half maximum FWHM, for evaporated CdTe and electrodeposited CdTe films.

AES and SIMS depth profiles of as-deposited films show moderately sharp interfaces at the CdTe–CdS and CdS–ITO surfaces. After the 400 °C heat treatment these measurements indicate that interdiffusion between CdTe, CdS, and $CdCl_2$ has occurred during the heat treatment: (1) interface are

TABLE 1

X-ray diffraction data for CdTe films before and after 400 °C heat treatment

Treatment	CdTe a_0 (Å)	I (111) (cps)	FWHM (111)
Evaporated			
As-deposited	6.490	940	0.35
HT 30 min	6.480	2500	0.18
HT 120 min	6.460	2000	0.18
Electrodeposited			
As-deposited	6.490	1000	0.20
HT 30 min	6.478	1850	0.16

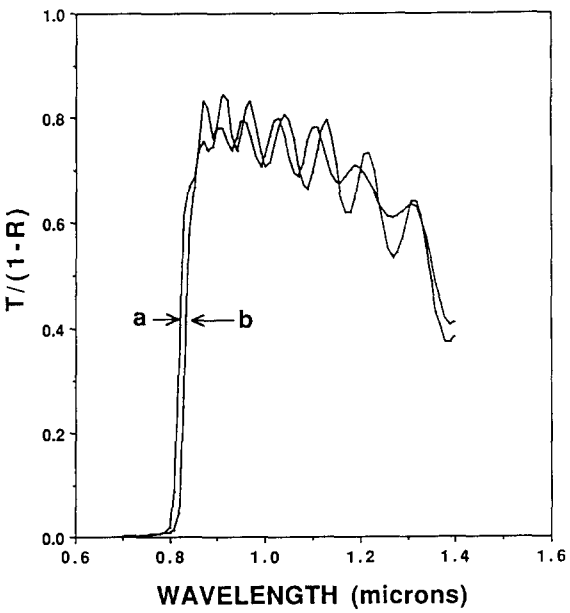

Fig. 2. T $(1 - R)^{-1}$ *vs.* wavelength for CdTe/CdS: (a) as-deposited; (b) after $CdCl_2$ coating and heat treatment at 400 °C in air for 30 min.

broadened considerably; (2) the sulfur level in CdTe increased 100 × above background; (3) the tellurium level in CdS increased 100 × above background; (4) the chlorine level throughout the structure increased by 10–100 × above background. The detection of sulfur in CdTe via pinholes or voids in CdTe is ruled out by cross-section SEM images which clearly indicate a densely packed columnar structure from ITO through CdTe. In addition to extensive interdiffusion of sulfur, tellurium and chlorine, a surface oxide was formed on the CdTe layer.

Figure 2 shows $T/(1\text{-}R)$ *vs.* wavelength for evaporated CdTe/CdS/ITO/7059 before and after $CdCl_2$/400 °C treatment. The sub-bandgap absorption

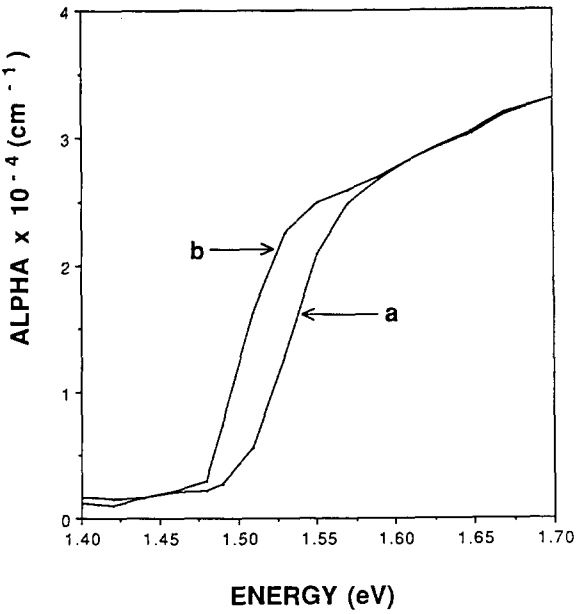

Fig. 3. Alpha *vs.* energy for CdTe/CdS: (a) as-deposited and (b) after $CdCl_2$ coating and heat treatment at 400 °C in air for 30 min.

in the as-deposited case (curve a) is due to free carrier absorption in the ITO layer. A shift in the optical absorption edge to lower energy after the 400 °C air heat treatment is apparent between curves a and b. From plots of α *vs.* energy (Fig. 3) before and after heat treatment the shift is approximately - 20 meV. No change in optical properties was observed on films heat treated at 400 °C without a $CdCl_2$ coating. However, heat treatment at >500 °C without $CdCl_2$ results in a similar shift in the absorption edge to samples heat treated with $CdCl_2$ at 400 °C.

All the above results, the shifts in lattice parameter and optical absorption edge, along with the AES and SIMS data, are consistent with the formation of a CdS_xTe_{1-x} layer [13–15]. Since the CdTe–CdS system is not isostructural at the temperatures involved (300–700 K), a phase transformation from zincblende to wurtzite occurs at composition $CdS_{0.2}Te_{0.8}$ [16]. A consequence of this is that the bandgap decreases with increasing sulfur content until $x=0.2$, at which the bandgap (E_g) reaches its minimum value of 1.3 eV [17]. Based on published values of E_g and a_0 as a function of x in CdS_xTe_{1-x}, the heat treated CdTe films contain 1–2 mol% sulfur.

3.2. Initial device results

Figures 4(a) and 5(a) show the initial *I–V* and *QE* characteristics for illumination through both the CdS and Cu/Au contact for a CdTe/CdS device. The initial V_{oc} is less than 400 mV, J_{sc} is less than 10 mA cm^{-2}, FF less than 40%, and the *I–V* curve has pronounced light-to-dark crossover. Quantum

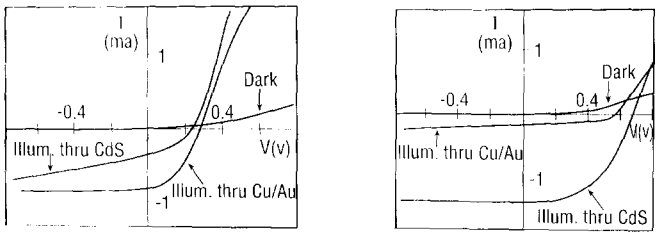

Fig. 4. *I–V* curves of CdTe/CdS devices: (a) after Cu/Au contact deposition and (b) after heat treatment at 150 °C in air for 2 h. The cell area was 0.08 cm^2.

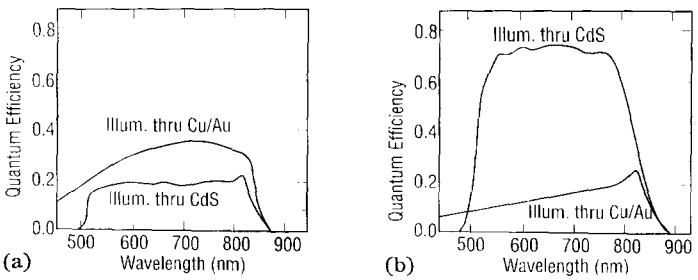

Fig. 5. *QE* curves of CdTe/CdS devices: (a) after Cu/Au contact deposition and (b) after heat treatment at 150 °C in air for 2 h.

efficiency measurements show nearly uniform collection independent of the illumination direction. For illumination through CdS, the response is limited at $\lambda < 500$ nm due to the CdS band edge.

Heat treatment at 150 °C

J_{sc} was optimized by air heat treatment at 150 °C for up to 2 h. No physical changes were seen in SEM or XRD, however AES profiles showed interdiffusion of the copper and gold layers. Figures 4(b) and 5(b) show the *I–V* and *QE* for illumination through CdS and Cu/Au. J_{sc} increased to 19 mA cm^{-2}, and V_{oc} increased to 670 mV for illumination through the CdS. The curvature in forward bias is due to non-ohmic behavior of the Cu/Au contact. The dark *J–V* characteristic was unchanged by the heat treatment. The quantum efficiency for illumination through the CdS increased uniformly while that for illumination through the Cu/Au contact decreased overall, with the maximum response near the CdTe adsorption edge. The quantum efficiency results suggest a shift from a p–i–n type junction (junctions at CdS/CdTe and CdTe/Cu/Au) to a p–n heterojunction between CdTe and CdS. Evolution from p–i–n to p–n behavior is consistent with the CdTe becoming more p-type throughout its bulk, probably resulting from diffusion of copper into the CdTe from the contact during the 150 °C heat treatment.

3.4. Chemical treatment

V_{oc} was optimized by immersion of the devices in either 0.01% Br_2–CH_3OH for 2–5 s or N_2H_4–H_2O for 2–5 min. This produced no noticeable change

in surface appearance, morphology, XRD spectrum, or optical properties. AES analysis, however, showed a decrease in cadmium near the surface. XPS analysis showed a drop in the Cd/Te peak area ratio from 1.9 to 0.4 with little change in copper content.

Figure 6 shows the *I–V* behavior for a device immersed in a bromine–methanol solution. This device had an efficiency of 9.6% with $V_{oc} = 729$ mV, $J_{sc} = 19$ mA cm^{-2}, and FF = 69%. The V_{oc} increased by 50 mV with no change in J_{sc} spectral response. We attribute the increase in V_{oc} to chemical interaction at the grain boundaries. The curvature in the forward bias portion of the *I–V* curves was eliminated by the treatment, resulting in little or no light-to-dark crossover. This results in increased FF due to a reduction in the series resistance. Removal of cadmium from the near-surface region of the contact produces excess tellurium which may react with copper, to form Cu_2Te, and with gold, forming ohmic contact with p-type CdTe [18]. Thus, the chemical treatment reduces J_0 in the device without changing the light-generated current (J_L) and improves the contact properties.

When the chemical treatment is performed prior to the 150 °C heat treatment, a moderate improvement in V_{oc} occurs but J_{sc} remains low and the quantum efficiency is similar to that in Fig. 5(a). The 150 °C heat treatment after the chemical immersion, however, does not improve the J_{sc} or change the spectral response. In this case, the chemical treatment has produced Cu_2Te thereby limiting the amount of free copper available to dope CdTe during the 150 °C heat treatment.

Applying the post-deposition, contacting, and optimization procedures described above to electrodeposited CdTe/CdS films produced devices with efficiencies greater than 10%. This demonstrates that CdTe layers deposited by two different techniques can be similarly optimized to give the same performance and shows the importance of post-deposition processing.

4. Conclusion

We have developed a simple contact and optimization process for making 10% efficient thin film CdS/CdTe devices using CdS and CdTe layers prepared by evaporation. By demonstrating high efficiency devices using CdTe and CdS deposited by evaporation and electrodeposition we have shown that the

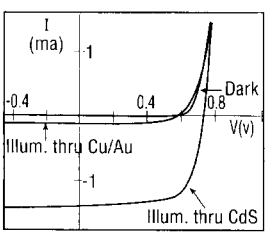

Fig. 6. *I–V* curves of CdTe/CdS device after heat treatment at 150 °C in air followed by immersion in Br_2–CH_3OH solution for 5 s.

CdTe and CdS deposition methods used are not critical to the fabrication of high efficiency devices. Instead, we find the post-deposition processing steps are more crucial to the performance of devices.

Heat treating CdTe with a $CdCl_2$ coating increases CdTe grain size and interdiffuses tellurium and sulfur. Without the $CdCl_2$ coating, higher CdTe growth temperatures (> 500 °C) or heat treatment temperatures are needed to produce these changes. Reproducible device results have been obtained using CdTe heat treated with $CdCl_2$.

Bifacial *I–V* and spectral response analyses show that initially the devices operate in a p–i–n type mode. After a mild heat treatment, which diffuses copper from the contact into the CdTe, the CdTe layer becomes more p-type, resulting in p–n device operation. Reaction of the CdTe–Cu/Au contact surface with Br_2–CH_3OH or N_2H_4–H_2O results in enhancement of V_{oc} and improvement of the contact. The relatively rapid effect of the chemical treatment suggests action through and along grain boundaries. AES and SIMS analyses indicate a sharp reduction in cadmium at the near-surface region of the CdTe which makes conditions favorable for formation of Cu_2Te. This makes ohmic contact to p-type CdTe, hence the improved fill factor.

Acknowledgments

The authors are grateful to the following people for their technical assistance in carrying our this work: Peter V. Meyers (formerly of AMETEK) for collaboration and electrodeposited samples; Sally Asher (SERI) and Art Nelson (SERI) for AES, SIMS, and XPS measurements; and Keith Emory (SERI) for efficiency measurements. We also wish to thank our colleagues at IEC, in particular Bill Baron, Jim Phillips, Sally Buchanan, Elaine Koronik, Ken Schubert, and Bill Shafarman. This work was supported by the Solar Energy Research Institute under Subcontract numbers XL-9-19032-1 and XN-0-10023-1.

References

1 Y.-S. Tyan and E. A. Perez-Albuerne, *Proc. 16th IEEE Photovoltaic Specialists' Conf.*, IEEE, New York, 1982, p. 794.
2 B. M. Basol, *Sol. Cells, 23* (1988) 69.
3 H. Matsumoto, K. Kuribayashi, H. Uda, Y. Komatsu, A. Nakano and S. Ikegami, *Sol. Cells, 11* (1984) 367.
4 T. L. Chu, *SERI Final Prog. Rpt. under Subcontract XL-3-03122-1*, 1985, Solar Energy Research Institute, Golden, CO. U.S.A.).
5 A. Rohatgi, S. A. Ringel, R. Sudharsanan, P. V. Meyers, C. H. Liu and V. Ramanathan, *Sol. Cells, 27* (1989) 219.
6 S. P. Albright, B. Ackerman, and J. F. Jordan, *IEEE Trans. Electron. Devices, ED-37* (1990) 434.
7 G. C. Morris, P. G. Tanner, and A. Tottszer, *Proc. 21st IEEE Photovoltaic Specialists' Conf.*, IEEE, New York, 1990, p. 575.

8 R. W. Birkmire, B. E. McCandless, and W. N. Shafarman, *Sol. Cells, 23* (1988) 115.
9 R. W. Birkmire, S. S. Hegedus, B. E. McCandless, J. E. Phillips, and W. N. Shafarman, *Proc. 19th IEEE Photovoltaic Specialists' Conf.*, IEEE, New York, 1987, p. 826.
10 P. V. Meyers, C.-H. Liu, and T. J. Frey, U.S. Patent 4 710 589 (1987).
11 C. S. Barrett and T. B. Massalski, *Structure of Metals*, Pergamon, New York, 1987.
12 A. Nelson and S. Asher, unpublished results, 1989.
13 D. Bonnet, *Phys. Stat. Sol., (a), 3* (1970) 913.
14 K. Ohata, J. Saraie and T. Tanaka, *Jpn. J. Appl. Phys., 12* (1973) 1198.
15 J. Saraie, H. Kata, N. Yamada, Sh. Kaida and T. Tanaka, *Phys. Stat. Sol. (a), 39* (1977) 331.
16 K. Ohata, J. Saraie and T. Tanaka, *Jpn. J. Appl. Phys., 12* (1973) 1641.
17 R. Hill and D. Richardson, *Thin Solid Films, 18* (1973) 25.
18 J. P. Ponpon, *Solid State Electron., 28* (1985) 689.